^{18}F-FDOPA Kinetics in Brain Tumors

Christiaan Schiepers[1], Wei Chen[1], Timothy Cloughesy[2], Magnus Dahlbom[1], and Sung-Cheng Huang[1]

[1]*Department of Molecular and Medical Pharmacology, David Geffen School of Medicine, University of California, Los Angeles, California; and* [2]*Department of Neurology, David Geffen School of Medicine, University of California, Los Angeles, California*

L-3,4-Dihydroxy-6-^{18}F-fluoro-phenyl-alanine (^{18}F-FDOPA) is an amino acid analog used to evaluate presynaptic dopaminergic neuronal function. Evaluation of tumor recurrence in neurooncology is another application. Here, the kinetics of ^{18}F-FDOPA in brain tumors were investigated. **Methods:** A total of 37 patients underwent 45 studies; 10 had grade IV, 10 had grade III, and 13 had grade II brain tumors; 2 had metastases; and 2 had benign lesions. After ^{18}F-DOPA was administered at 1.5–5 MBq/kg, dynamic PET images were acquired for 75 min. Images were reconstructed with iterative algorithms, and corrections for attenuation and scatter were applied. Images representing venous structures, the striatum, and tumors were generated with factor analysis, and from these, input and output functions were derived with simple threshold techniques. Compartmental modeling was applied to estimate rate constants. **Results:** A 2-compartment model was able to describe ^{18}F-FDOPA kinetics in tumors and the cerebellum but not the striatum. A 3-compartment model with corrections for tissue blood volume, metabolites, and partial volume appeared to be superior for describing ^{18}F-FDOPA kinetics in tumors and the striatum. A significant correlation was found between influx rate constant K and late uptake (standardized uptake value from 65 to 75 min), whereas the correlation of K with early uptake was weak. High-grade tumors had significantly higher transport rate constant k_1, equilibrium distribution volumes, and influx rate constant K than did low-grade tumors ($P < 0.01$). Tumor uptake showed a maximum at about 15 min, whereas the striatum typically showed a plateau-shaped curve. Patlak graphical analysis did not provide accurate parameter estimates. Logan graphical analysis yielded reliable estimates of the distribution volume and could separate newly diagnosed high-grade tumors from low-grade tumors. **Conclusion:** A 2-compartment model was able to describe ^{18}F-FDOPA kinetics in tumors in a first approximation. A 3-compartment model with corrections for metabolites and partial volume could adequately describe ^{18}F-FDOPA kinetics in tumors, the striatum, and the cerebellum. This model suggests that ^{18}F-FDOPA was transported but not trapped in tumors, unlike in the striatum. The shape of the uptake curve appeared to be related to tumor grade. After an early maximum, high-grade tumors had a steep descending branch, whereas low-grade tumors had a slowly declining curve, like that for the cerebellum but on a higher scale.

Key Words: ^{18}F-FDOPA; PET; brain tumors; kinetic modeling; factor analysis

J Nucl Med 2007; 48:1651–1661
DOI: 10.2967/jnumed.106.039321

Imaging of glucose utilization is a routine diagnostic procedure in the evaluation of cancer. Imaging of brain tumors with labeled amino acids or analogs, such as methionine, tyrosine, leucine, alanine, and isobutyric acid, has been reported (*1–5*). An evaluation of cellular proliferation in brain gliomas with ^{18}F-fluorothymidine in comparison with ^{18}F-FDG was published earlier (*6*). Kinetic modeling of ^{18}F-fluorothymidine in brain tumors was reported elsewhere (*7*).

The clinical application of L-3,4-dihydroxy-6-^{18}F-fluoro-phenyl-alanine (^{18}F-FDOPA) in brain tumors has been reported as a case report (*1*), as a clinical study (*5*), and from our institution (*8*). Chen et al. (*8*) showed that high ^{18}F-FDOPA uptake was a predictor of tumor recurrence, and tumor uptake higher than uptake in the striatum had overall sensitivity of 92% and specificity of 95% for recurrence. The main advantage of ^{18}F-FDOPA was with low-grade tumors, which showed higher uptake of ^{18}F-FDOPA than of ^{18}F-FDG, with mean standardized uptake values (SUVs) of 2.5 and 1.2, respectively.

The kinetics of ^{18}F-FDOPA in the striatum and cerebellum of volunteers were investigated by Huang et al., and a model for the human brain was published (*9*). In the present study, we investigated the kinetics in brain gliomas, brain metastases, and benign lesions. The tracer kinetics were studied with image-derived time–activity curves, that is, tracer clearance from the vascular space and uptake in the striatum, the cerebellum, and tumors. Kinetic modeling was used to estimate the rate constants for the various compartments. Two- and 3-compartment models were tested, and Patlak (*10*) and Logan (*11*) graphical analyses were evaluated. Metabolite and partial-volume corrections were applied to estimate ^{18}F-FDOPA transport across the blood-brain barrier (BBB) and ^{18}F-FDOPA influx into brain tissues or tumors.

MATERIALS AND METHODS

Patients

The study population consisted of 37 patients, 33 with primary brain tumors, 2 with brain metastases from somatic cancers, and 2

Received Dec. 25, 2006; revision accepted Jun. 27, 2007.
For correspondence contact: Christiaan Schiepers, Department of Molecular and Medical Pharmacology, David Geffen School of Medicine at UCLA, AR-144 CHS, 10833 Le Conte Ave., Los Angeles, CA 90095-6942.
E-mail: cschiepers@mednet.ucla.edu

with benign lesions. There were 21 men and 16 women, with an average age of 45 y (range, 20–69 y). The study was approved by the local Office for Protection of Research Subjects (Institutional Review Board), and all patients gave written informed consent to participate in the imaging study. Nine patients had newly diagnosed tumors, and 24 had recurrences. Histopathologic analysis revealed glioblastoma multiforme ($n = 10$; World Health Organization [WHO] grade IV), anaplastic oligodendroglioma ($n = 7$; WHO grade III), anaplastic oligoastrocytoma ($n = 3$; WHO grade III), astrocytoma ($n = 5$; WHO grade II), oligoastrocytoma ($n = 3$; WHO grade II), oligodendroglioma ($n = 5$; WHO grade II), lung cancer metastasis ($n = 1$); and melanoma metastasis ($n = 1$). Six of these 35 patients had tumors with predominantly posttreatment changes detected by clinical follow-up and imaging (range, 2–5 y) and were analyzed as a separate group. Two patients had benign lesions: one had gliosis, and one had no pathologic diagnosis but had normal 3-y follow-up MRI and PET results. Four of the 33 patients with primary brain tumors had repeat studies, and 2 had 2 repeat studies, amounting to a total of 45 studies. Thus, 45 time–activity curves were available for the striatum and the cerebellum. Eleven patients had multiple tumor locations; thus, 61 separate malignant tumor time–activity curves and 2 benign lesion time–activity curves could be analyzed.

Acquisition

^{18}F-FDOPA was synthesized according to a previously reported procedure (*12*). An ^{18}F-FDOPA dose of 1.5–5 MBq/kg (0.05–0.15 mCi/kg) was administered intravenously.

PET imaging was performed with an ECAT HR+ system (CTI/Siemens). A transmission scan of 5-min duration was acquired first, in the 2-dimensional mode. Subsequently, ^{18}F-FDOPA was administered intravenously, and a dynamic acquisition was started. The emission scan was acquired in the 3-dimensional mode. A total of 26 frames were acquired at 8×15 s, 2×30 s, 2×60 s, and 14×300 s. The images were reconstructed with iterative techniques: maximum a posteriori maximization (*13*) for the transmission scan and ordered-subset expectation maximization consisting of 6 iterations with 8 subsets (*14*) for the emission scan. Corrections for attenuation and scatter were applied. A gaussian kernel with a 5-mm full width at half maximum was used as a postreconstruction smoothing filter. The final volume set had a matrix size of 128×128 and consisted of 63 planes, resulting in a voxel size of $2.45 \times 2.45 \times 2.425$ mm^3.

Processing

Factor analysis (FA) was performed on the reconstructed images (*15*). To speed up processing, data were resampled into larger voxels. Zooming, summation of planes, and rebinning produced an isometric dataset of $4.9 \times 4.9 \times 4.9$ mm^3 voxels that was used for further processing. Time–activity curves were generated for every voxel within the head contour. Each time–activity curve could be represented as a vector in a multidimensional space. FA with a positivity constraint was performed on the vector set. For our implementation, 3 factors and their corresponding images (factor images) were generated. Factor 1 represents the venous structures, factor 2 represents the striatum, and factor 3 represents the remainder. The tumor was usually seen in factor 2 images and, if not, was found in factor 3 images. FA could not separate the arterial vessels from the venous vessels (sampling of 15 s). The ^{18}F-FDOPA extraction was low, and the arterial-venous difference was small; therefore, our input function was a close approximation of a local arterial blood curve. Simple threshold techniques were used to create a volume of interest (VOI) from the corresponding factor image. For the transverse sinuses, a threshold of 50% was used (the usual at our institution), and for tumors, 75% was used to exclude any potential necrotic zones. The threshold for the striatum was also set at 75%, whereas that for the cerebellum was set at 67%.

With the created VOIs and the reconstructed dynamic dataset, image-based time–activity curves were generated. The time–activity curve for the transverse sinuses served as the blood curve. The time–activity curves for tumors, the striatum, and the cerebellum were used for kinetic modeling. For patients with tumors close to the striatum, the contralateral basal ganglion was used for the striatal time–activity curve to avoid possible adverse effects (such as tumor infiltration or a radiation or chemotherapy response) on the ipsilateral part of the striatum.

Compartmental Model

The model for ^{18}F-FDOPA kinetics, based on known biochemical pathways, was described elsewhere (Fig. 1). In the approach of Huang et al. (*16*), a 3-compartment model is used for the striatum and a 2-compartment model is used for the cerebellum. This model is complex, uses 2 input functions, both measured with blood sampling, and needs extra constraints to achieve convergence and acceptable variability in the parameter estimates. The model of Huang et al. (*16*) is not practical clinically, and a simpler approach is desirable for routine applications. For the present study, the kinetic model was adapted to the standard 3-compartment model that is generally used for ^{18}F-FDG (*17,18*). The same model is proposed for striatal, neoplastic, and cerebellar tissues, and exactly the same model structure was used. In brief, the model assumes the transport of ^{18}F-FDOPA from the vascular space to the tissue space. No partitioning is considered in the vascular

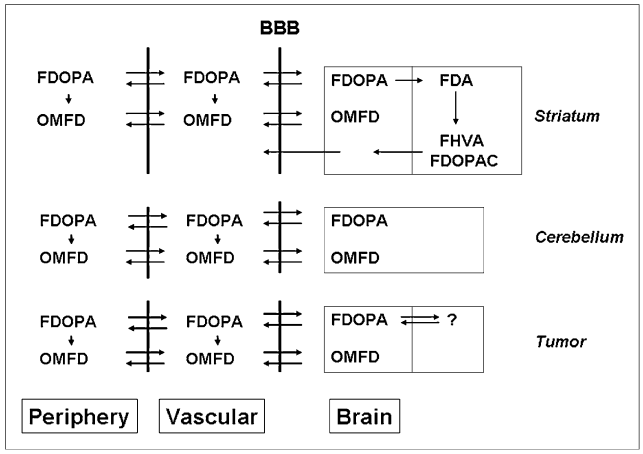

FIGURE 1. Biochemical pathways of ^{18}F-FDOPA after administration in venous circulation. Metabolite OMFD is produced in blood and liver and in negligible amounts in brain and is transported bidirectionally. Because this metabolite still has ^{18}F label, it cannot be distinguished from injected tracer ^{18}F-FDOPA. In brain, 2 compartments are considered: one with unbound ^{18}F-FDOPA and another with bound (metabolized) tracer. Question mark indicates that role of ^{18}F-FDOPA in third compartment of tumors is not known. FDA = 6-fluorodopamine; FDOPAC = 6-fluoro-3,4-dihydroxyphenylacetic acid; FHVA = 6-fluorohomovanillic acid. Adapted from Huang et al. (*16*).

space; plasma and blood activity concentrations are the same after 5 min (see Fig. 3 in the article by Huang et al. (*16*)). ^{18}F-FDOPA is transported between plasma and tissue through amino acid channels (*19*). In the tissue space, there is an exchangeable compartment (with unbound ^{18}F-FDOPA) and a compartment with bound ^{18}F-FDOPA. In addition, ^{18}F-FDOPA is metabolized in the body tissues and in the liver to L-3,4-dihydroxy-6-fluoro-3-*O*-methylphenylalanine (OMFD), which can cross the BBB bidirectionally (*20*). Metabolism of ^{18}F-FDOPA to OMFD inside the brain is negligible, as demonstrated by Huang et al. (*9,16*). In the striatum, ^{18}F-FDOPA is converted to 6-fluorodopamine, represented by the third compartment. Whereas the third compartment is well defined for the striatum, it is not for tumors, as indicated by the question mark in Figure 1.

The effects of corrections for tissue blood volume, metabolites, and partial volume were investigated. Kinetic modeling with 3 compartments yielded 4 rate constants (k_1, k_2, k_3, and k_4) from which the influx rate constant K was calculated as $(k_1 \times k_3)/(k_2 + k_3)$. The blood volume fraction in tissue was estimated as a fifth parameter. Patlak graphical analysis was performed by use of an input function without metabolite correction to estimate the influx rate constant K_{patlak}. A 2-compartment model was also tested by merging compartments 2 and 3 and estimating 2 rate constants and the blood volume fraction in tissue.

In the present study, no metabolites were measured; instead, data from an earlier publication (*16*) were retrieved. As reported previously, carbidopa blocks the peripheral decarboxylation of ^{18}F-FDOPA almost completely (*9,16*). In that situation, only the metabolite OMFD needs to be considered; other, peripheral, metabolites (MET) are negligible (*9*). The serum metabolites of volunteers who received pretreatment with carbidopa were pooled and fitted with a theoretic curve, which appeared to provide a good approximation of OMFD in the blood. At 2 h, OMFD comprised approximately 82% of the activity in the vascular compartment (*16*). For our experiments, a monoexponential function was used:

$$\text{OMFD fraction} = 0.84 \times (1 - e^{-0.028 \times T}). \quad \text{Eq. 1}$$

In this equation, time (T) is given in minutes after injection.

In our population, one third of the patients were studied with 200 mg of carbidopa given orally 1 h before ^{18}F-FDOPA administration, but two thirds of the patients were studied without premedication. For this group, MET could not be ignored. The MET fraction was estimated by use of data from earlier work (*9*), which were fitted with a biexponential function:

$$\text{MET fraction} = [0.6 \times (1 - e^{-0.08 \times T})] - 0.1 \times e^{+0.01 \times T}. \quad \text{Eq. 2}$$

The 2 groups of patients were analyzed with different metabolite corrections: only OMFD for cases in which carbidopa pretreatment was used and both OMFD and MET for all other cases.

The distribution volume for free ^{18}F-FDOPA was calculated as $k_1/(k_2 + k_3)$, and the equilibrium distribution volume was calculated as k_1/k_2. To investigate the distributions of ^{18}F-FDOPA and metabolites in more detail, Logan graphical analysis was performed (by use of an input function consisting of ^{18}F-FDOPA and OMFD). The cerebellum shows no specific binding of ^{18}F-FDOPA and OMFD, which are transported through large neutral amino acid channels and, in some cases, the sodium-dependent transport systems in the BBB.

The recovery coefficient for converting the transverse sinus time–activity curve to the input function was 0.7 for our PET system (*7*). The tumors were at least 15 mm; the recovery coefficient for tumors, the striatum, and the cerebellum was set to unity to obtain the output function. Partial-volume correction affects only k_1 and, therefore, the influx rate constant K, the distribution volume, and the equilibrium distribution volume.

Statistical Analysis

Group results are presented as mean ± SD. The Student *t* test was used to compare the kinetic parameters and ^{18}F-FDOPA uptake between subgroups. For small sample sizes ($n < 10$), the Wilcoxon–Mann-Whitney *U* test (2-sample rank test) was applied. Pearson correlation and linear regression analyses were used to study the correlations among subgroups, tumor types, and patients. Differences between kinetic models were analyzed with the F test to correct for the different numbers of parameters involved in the various models (*21,22*).

RESULTS

In Figure 2A, typical images are displayed for factor 1, representing the vascular structures, for example, the transverse and cavernous sinuses. Figure 2B shows the images of a right frontal tumor, and Figure 2C shows the images of the striatum. In general, tumors and the striatum were visualized in the same factor image (factor 2). This finding indicated that the temporal behavior of ^{18}F-FDOPA was similar for tumors and the striatum. In 7 studies (5 patients), tumors were not seen in factor 2 images, indicating that these tumors had a temporal pattern different from that of the striatum. In 10 studies (7 patients), tumors were seen in 2 types of factor images, that is, factor 2 and factor 3; in another patient, with 3 tumor locations, one tumor was represented in both factor 2 and factor 3 images. The latter finding suggests that these tumors had 2 different uptake patterns. VOIs were created from the factor images, and time–activity curves were generated; typical examples of uptake curves are shown in Figure 3.

Striatal ^{18}F-FDOPA Kinetics

The kinetic parameters of the striatum are shown in Table 1. The 2-compartment model using an input function without metabolite correction failed, as expected. The fits between the model-generated curve and measured points were not tight. A 3-compartment model produced superior results. Metabolite correction resulted in a better fit of the time–activity curves. As an error estimate, the weighted residual sum of squares (WRSS) was used (Table 1). WRSS was calculated as follows:

$$\text{WRSS} = \sum_{i=1}^{26} (Y_i^{\text{fitted}} - Y_i^{\text{measured}})^2 \times (\text{duration of frame i}/\text{maximum frame duration}), \quad \text{Eq. 3}$$

where Y_i^{fitted} is the radioactivity concentration in frame i calculated with kinetic modeling and Y_i^{measured} is the

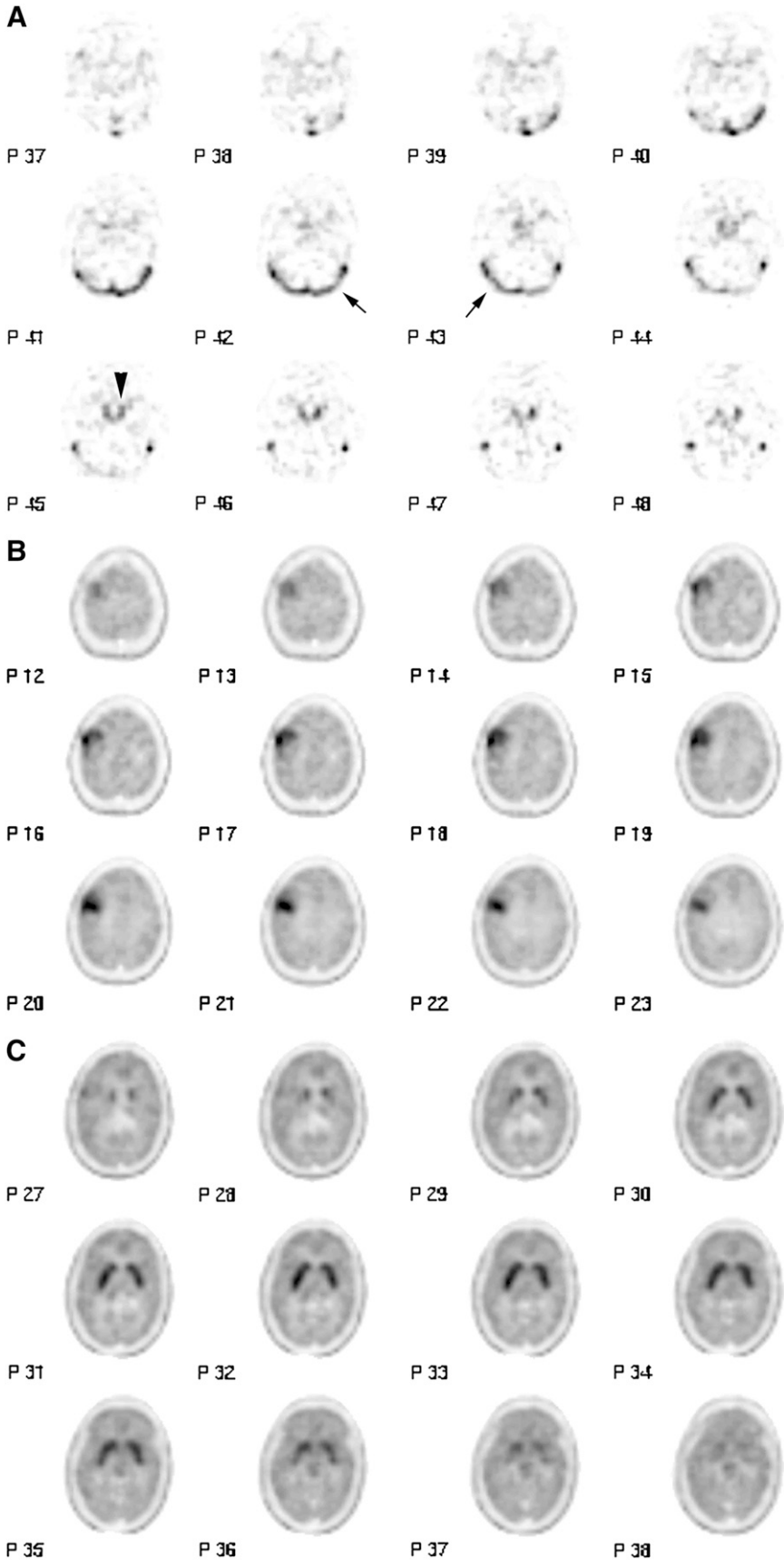

FIGURE 2. Factor images for 24-y-old woman with newly diagnosed brain tumor. Pathology revealed grade III oligodendroglioma. (A) Vascular factor images of transverse (arrows) and cavernous (arrowhead) sinuses. (B) Factor images of tumor located in right frontal lobe. (C) Striatum with some asymmetry in caudate nucleus and globus pallidus because of head tilt. Note inferior edge of right frontal tumor in plane P 27.

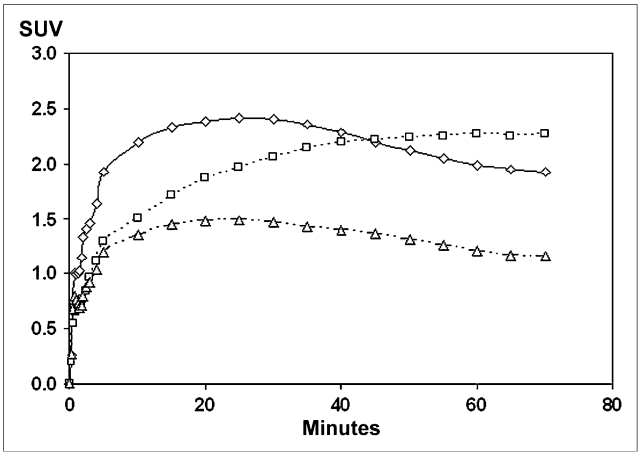

FIGURE 3. Typical time–activity curves for striatum (□), cerebellum (△), and tumor (◇). Maximum uptake in tumor was higher than that in striatum. Note early steep ascent in tumor curve and parallel patterns of tumor and cerebellum curves. In contrast, striatum had active metabolism, leading to plateau-shaped curve.

radioactivity concentration in frame i measured by the PET scanner. A dramatic decrease in the error estimate was observed when a 3-compartment model was used instead of a 2-compartment model, revealing highly significant differences ($P < 0.01$, as determined by an F test) for every patient (Table 1). Corrections for metabolites and partial volume further improved the fits and reduced the error estimates (Table 1). A comparison of no metabolite correction and metabolite correction revealed significantly different ($P < 0.01$) error estimates (Table 1). An additional model was tested by fixing k_4 at zero; this model yielded generally lower estimates, except for the distribution volume. Finally, graphical analysis was performed with Patlak and Logan plots. The influx rate constant K_{patlak} was significantly lower than the influx rate constant K estimated by compartmental modeling; Logan plots produced reliable estimates of the distribution volume. From these analyses, it is clear that a 3-compartment model with metabolite correction is necessary to describe ^{18}F-FDOPA kinetics in the striatum.

Tumor Kinetic Model

The same model structures as those used for the striatum were investigated and compared for tumors (Table 2). Visual inspection of the curves revealed that tumors could be fitted with a 2-compartment model. Moving from a 2-compartment model to a 3-compartment model decreased the error estimates and improved the goodness of fit. The error estimates obtained with the 2-compartment and 3-compartment models were significantly different for 48 of 61 tumors ($P < 0.05$, as determined by an F test (*21,22*)). Group comparisons showed the error estimates to be significantly smaller for the 3-compartment model than for the 2-compartment model ($P < 0.01$, as determined by a sign test). When metabolite correction was not applied, values for the influx rate constant K were consistently—that is, for each tumor in every patient—lower ($P < 0.01$, as determined by a sign test).

The average results for the striatum, tumors, and the cerebellum are shown in Figure 4. In general, tumors had the highest transport rate, the cerebellum had the lowest transport rate, and the striatum had an intermediate transport rate. Detailed inspection revealed significant differences between the striatum and tumors for all parameters ($P < 0.001$) except k_2 ($P = 0.3$). The striatum–cerebellum comparison revealed significant differences for all parameters ($P < 0.001$). Comparison of the cerebellum and

TABLE 1
Kinetic Modeling of Striatum*

Parameter	2C-3p	3C-5p	3C-5p	3C-4p with $k_4 = 0$	Patlak-2p	Logan-2p
Metabolite correction	No	No	Yes	Yes	No	No
k_1	0.108 ± 0.023	0.163 ± 0.044	0.124 ± 0.034	0.088 ± 0.020		
k_2	0.052 ± 0.007	0.165 ± 0.072	0.199 ± 0.084	0.084 ± 0.024		0.047 ± 0.007
k_3		0.029 ± 0.017	0.075 ± 0.019	0.034 ± 0.004		
k_4		0.014 ± 0.011	0.010 ± 0.004			
K		0.023 ± 0.009	0.034 ± 0.008	0.025 ± 0.005	0.015 ± 0.003	
V_b	0.01 ± 0.01	0.14 ± 0.05	0.10 ± 0.03	0.12 ± 0.03		
V_{ed}	2.09 ± 0.41	1.10 ± 0.39	0.69 ± 0.23	1.12 ± 0.36	1.28 ± 0.26	1.61 ± 0.31
WRSS	1,811 ± 823	178 ± 137	150 ± 98	229 ± 128		
n ($P < 0.05$)	Reference	45	45	45		

*Estimates of fitted parameters k_1–k_4, influx rate constant K, blood volume fraction in tissue (V_b), and equilibrium distribution volume (V_{ed}) were determined. Results are expressed as mean ± SD for 45 studies in 37 patients. Partial-volume correction was applied. Input function was corrected for metabolites as indicated. Error estimate WRSS was measure of goodness of fit between measured and calculated output functions. Graphical analysis with Patlak and Logan plots was applied to images obtained between 15 and 75 min. *n* ($P < 0.05$) denotes number of studies with significantly lower error than 2C-3p (reference), as determined by F test.

2C = 2-compartment model; 3p = 3 parameters; 3C = 3-compartment model; 5p = 5 parameters; 4p = 4 parameters; 2p = 2 parameters.

TABLE 2
Kinetic Modeling of Tumors*

Parameter	2C-3p	3C-5p	3C-5p	3C-4p with $k_4 = 0$	Patlak-2p	Logan-2p
Metabolite correction	No	No	Yes	Yes	No	No
k_1	0.347 ± 0.399	0.271 ± 0.259	0.225 ± 0.179	0.206 ± 0.178		
k_2	0.219 ± 0.188	0.205 ± 0.134	0.169 ± 0.077	0.129 ± 0.073		0.143 ± 0.495
k_3		0.003 ± 0.004	0.031 ± 0.019	0.014 ± 0.005		
k_4		0.011 ± 0.025	0.016 ± 0.011			
K		0.003 ± 0.004	0.028 ± 0.016	0.017 ± 0.007	0.001 ± 0.006	
V_b	0.03 ± 0.02	0.15 ± 0.10	0.18 ± 0.11	0.18 ± 0.11		
V_{ed}	1.44 ± 0.56	1.23 ± 0.52	1.27 ± 0.58	1.52 ± 0.65	2.10 ± 0.89	1.53 ± 0.57
WRSS	2,370 ± 3,372	1,632 ± 3,512	470 ± 685	903 ± 1,657		
n ($P < 0.05$)	Reference	22	48	33		

*Estimates of fitted parameters k_1–k_4, influx rate constant K, blood volume fraction in tissue (V_b), and equilibrium distribution volume (V_{ed}) were determined. Results are expressed as mean ± SD for 61 malignant tumors in 35 patients. Same model structures and corrections as those described in Table 1 were tested. See Table 1 for definitions of abbreviations as well.

tumors yielded significant differences for all parameters ($P < 0.001$) except k_4 ($P = 0.7$). Thus, a 3-compartment model with correction for metabolites improves fit, reduces errors, and appears to be the best model for describing ^{18}F-FDOPA kinetics in tumors.

Tumor Kinetics and Grade

Tumors were classified as high grade, low grade, or metastatic according to their pathology. From a clinical perspective, tumors could be categorized with respect to their biologic behavior as newly diagnosed tumors (9 patients, 16 tumors), recurrent tumors (18 patients, 35 tumors), tumors with predominantly posttreatment changes (6 patients, 10 tumors), and benign lesions (2 patients, 2 lesions). Figure 5 shows the kinetic parameters for the tumor types; the data suggested that high-grade tumors had the highest transport rate constant k_1, whereas tumors with posttreatment changes tended to have the lowest. The other parameters did not show specific trends, although k_3 appeared to be somewhat higher for tumors with predominantly posttreatment changes. Statistically significant differences ($P < 0.01$) for k_1 and distribution volume were found between newly diagnosed high-grade tumors and low-grade tumors and between newly diagnosed high-grade tumors and tumors with predominantly posttreatment changes (Fig. 5). No statistically significant differences were found between low-grade tumors and tumors with predominantly posttreatment changes.

The uptake in the upper quartile of voxels (from 75% to 100%) was used to calculate the SUV. Because ^{18}F-FDOPA uptake usually has an early maximum, we calculated an early SUV (SUV_{early}; from 15 to 25 min) and a late SUV (SUV_{late}; from 65 to 75 min). The average value for SUV_{early} was 2.32, and that for SUV_{late} was 1.44; the differences were statistically significant ($P < 0.001$). Pearson coefficients of correlation with the influx rate

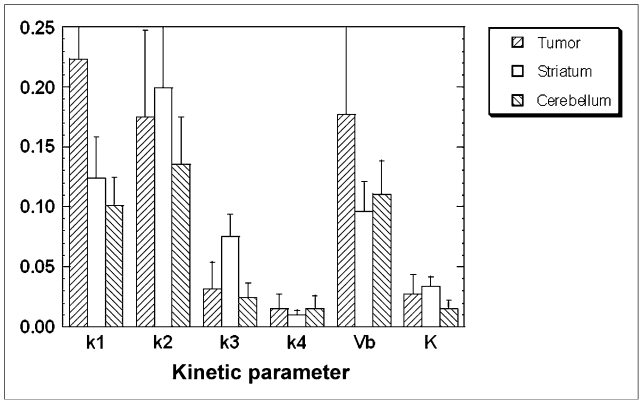

FIGURE 4. Kinetic parameters obtained with 3-compartment model and corrections for metabolites and partial volume. Average results for 45 studies of different structures are shown. Error bars denote SDs. Only one malignant tumor was selected per patient. Values for k_1–k_4 and K are given in minutes^{-1}. V_b = blood volume fraction in tissue.

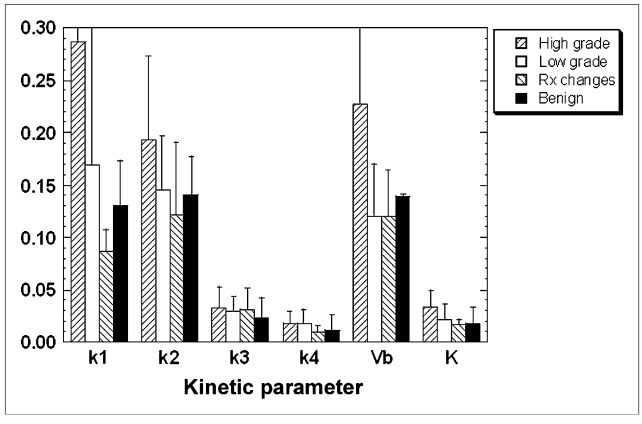

FIGURE 5. Average values of kinetic parameters for high-grade tumors ($n = 18$), low-grade tumors ($n = 11$), tumors with predominantly posttreatment (Rx) changes ($n = 6$), and benign lesions ($n = 2$) in brain. Error bars denote SDs. Values for k_1–k_4 and K are given in minutes^{-1}. V_b = blood volume fraction in tissue.

constant K were 0.44 for SUV_{early} and 0.71 for SUV_{late}. Significant differences for SUV_{early} and SUV_{late} were found between newly diagnosed high-grade tumors and low-grade tumors, between newly diagnosed high-grade tumors and tumors with posttreatment changes, and between recurrent tumors (both high grade and low grade) and tumors with posttreatment changes. No differences were found between newly diagnosed low-grade tumors and tumors with predominantly posttreatment changes, which had, overall, the lowest ^{18}F-FDOPA uptake.

The ranges of rates of transport across the BBB appeared to be similar for high-grade and low-grade tumors and types, whereas tumors with predominantly posttreatment changes had a limited range, up to 0.2 min^{-1}. No correlation was found with the influx rate constant K. This finding suggested that K for ^{18}F-FDOPA and, therefore, SUV_{late} were not dependent on transport rates for the different tumor types and grades. There were great variations in k_1, with a large degree of scatter, but the regression lines for k_1 versus K had a slope of zero for each tumor type, that is, high-grade tumors, low-grade tumors, and tumors with predominantly posttreatment changes.

Patlak graphical analysis carried out with images obtained between 15 and 75 min after injection and an input function without metabolite correction furnished a K_{patlak} value for malignant tumors that had a weak correlation with the influx rate constant K ($r = 0.56$ with metabolite correction and $r = 0.54$ without). The mean K_{patlak} value (mean, 0.001) was significantly different ($P < 0.001$) from the K value (0.028 with metabolite correction and 0.004 without). The low value for K_{patlak} indicated that ^{18}F-FDOPA and OMFD were not specifically sequestered in tumors and that Logan graphical analysis was more appropriate.

Two patients in the group that had tumors with predominantly posttreatment changes had a stable clinical course; they were studied 1 y apart without any intervening treatment. The first study was performed 1 h after the oral administration of 200 mg of carbidopa, and the second study was performed without any premedication. After carbidopa pretreatment, early uptake increased by 1.3–1.7 times and late uptake increased by 1.6–1.8 times relative to uptake in the study without pretreatment. These changes were seen for all structures—the striatum, the cerebellum, and tumors. On average, pretreatment with carbidopa increased early uptake by 50% and late uptake by 70%.

Distribution Volumes for ^{18}F-FDOPA and OMFD

Newly diagnosed tumors were not subjected to any therapy and constituted a "naive" subgroup. Of the patients with such tumors, 4 had high-grade tumors and 5 had low-grade tumors. In Figure 6, the equilibrium distribution volumes are plotted for both 2- and 3-compartment models, and separation by tumor grade was obtained. These results indicated that high-grade tumors had a higher distribution volume and, therefore, higher uptake of ^{18}F-FDOPA than did low-grade tumors. The clear separation of the 2 groups

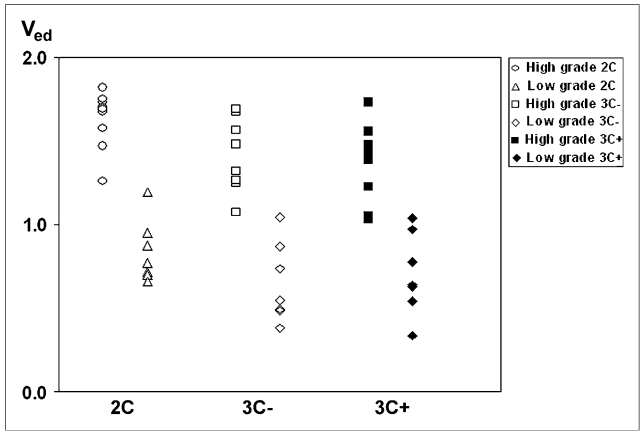

FIGURE 6. Plot of equilibrium distribution volume ($V_{ed} = k_1/k_2$) for newly diagnosed tumors. High- and low-grade tumors formed separate subgroups. High grade: 4 patients with 9 tumors. Low grade: 5 patients with 7 tumors. 2C = 2-compartment model; 3C− = 3-compartment model without metabolite correction; 3C+ = 3-compartment model with metabolite correction.

by the 2-compartment model and the 3-compartment model without metabolite correction suggested that the ^{18}F label measured by the PET scanner, that is, the total amount of ^{18}F-FDOPA plus OMFD, moved into the tumor and washed out as a function of time. Correction for metabolites, that is, considering ^{18}F-FDOPA accumulation alone, revealed a minor overlap; overall, however, the separation of the equilibrium distribution volumes between high- and low-grade tumors was maintained (Fig. 6).

Logan graphical analysis (using an input function without metabolite correction) was applied, and the average distribution volumes for the striatum and malignant tumors are given in Tables 1 and 2, respectively. For malignant tumors, the Pearson correlation coefficients for the distribution volume calculated by Logan graphical analysis and the equilibrium distribution volumes calculated by other models were 0.99 (2-compartment model with 3 parameters), 0.99 (3-compartment model with 5 parameters and without metabolite correction), and 0.92 (Patlak graphical analysis).

The Logan graphical analysis results obtained for the 2 patients with a stable clinical course and with or without carbidopa pretreatment are shown in Table 3 for the cerebellum. An excellent correspondence was found between the distribution volume with pretreatment and the distribution volume without pretreatment after correction for the MET fraction. These results suggested that Logan graphical analysis yielded reliable estimates of the distribution volume for ^{18}F-FDOPA plus OMFD after application of the appropriate correction.

Table 4 shows the distribution volumes for tumors in the patients with and the patients without carbidopa pretreatment and the corresponding metabolite corrections. There was good agreement between the compartment models and

TABLE 3
Equilibrium Distribution Volumes (V_{ed}) for Cerebellum in Patients With and Without Oral Pretreatment With 200 mg of Carbidopa*

		With carbidopa pretreatment		Without carbidopa pretreatment	
Patient	Model	Study	V_{ed}	Study	V_{ed}
A	2C-3p	1	**1.49**	2	1.98
	2C-3p+			2	**1.21**
	Logan	1	**1.14**	2	1.88
	Logan+			2	**1.16**
B	2C-3p	1	**1.08**	2	1.77
	2C-3p+			2	**1.03**
	Logan	1	**1.11**	2	1.82
	Logan+			2	**1.21**

*Values were obtained with 2-compartment model (2C) with 3 parameters (3p) or Logan graphical analysis. + indicates that MET correction was applied to input function (Eq. 2). Effect of peripheral MET correction is shown in last column. Bold type indicates directly comparable conditions.

the Logan plots within each patient group. Correction for the MET fraction increased the distribution volume in the patients who were not pretreated to values just above those in the patients who were pretreated, and the differences between the groups were not significant ($P > 0.1$).

^{18}F-FDOPA Uptake Patterns

The striatal time–activity curve showed an initial incline that approached a plateau, reaching the maximum, on average, at 37.5 min, as expected. Analysis of the individual tumor time–activity curves revealed that the early maximum values in tumor uptake occurred at 12.7 min (high-grade tumors), 15.7 min (low-grade tumors), and 19.6 min (tumors with predominantly posttreatment changes). The maximum for metastases occurred at 20 min, and that for benign lesions occurred at 15 min. In general, high-grade tumors showed a higher maximum (mean SUV_{early}, 2.64) followed by a rapid decline (mean SUV_{late}, 1.55), whereas low-grade tumors showed a lower maximum (mean SUV_{early}, 1.99) followed by a slower decline (mean SUV_{late}, 1.25). The time–activity curve for low-grade tumors resembled that for the cerebellum (Fig. 2C). The sharp decline seen for high-grade tumors was never observed for the cerebellum.

DISCUSSION

In the present study, the kinetics of ^{18}F-FDOPA in brain tumors were investigated, and a 3-compartment model appeared to describe the data best. Our method of analysis is completely image based and virtually operator independent. FA takes all voxels within the head contour into account. The factor images are parametric images, yielding the structures of interest. The threshold algorithm automatically creates the VOI in the *x*-, *y*-, and *z*-dimensions from the factor image. The VOIs are used to generate the time–activity curves from the dynamic dataset. In the past, we demonstrated that FA can reliably generate an input function for various radiopharmaceuticals and organ systems (*15,23–25*). These studies showed that kinetic parameters obtained with an FA-based input function are very similar to those obtained with a sampled blood curve, and no statistically significant differences were found for the rate constants obtained with these time–activity curves. Corrections for tissue blood volume, metabolites, and partial volume are necessary to produce adequate fits between the measured and the model-generated time–activity curves. We did not measure individual metabolites but used data from an earlier study (*16*).

The compartmental model used in the present study to describe ^{18}F-FDOPA kinetics in brain tissues is a simplified form adapted to the clinical environment. Therefore, the values of the rate constants cannot be compared directly with those from the full ^{18}F-FDOPA model (*16*), and the meaning of some rate constants is quite different. For example, k_3 in the simplified model does not necessarily represent the decarboxylation of ^{18}F-FDOPA to 6-fluorodopamine. Because tissue contains OMFD, which is a product of ^{18}F-FDOPA converted peripherally and transported from plasma, it will be reflected as a non-zero k_3 value when the simplified model is used along with the metabolite-corrected input function. In fact, the k_3 value obtained for the cerebellum with the

TABLE 4
Equilibrium Distribution Volumes (V_{ed}) for Tumors in Patient Groups With and Without Oral Pretreatment With 200 mg of Carbidopa*

	With carbidopa pretreatment			Without carbidopa pretreatment		
Model	No. of patients	No. of tumors	V_{ed}	No. of patients	No. of tumors	V_{ed}
2C-3p	12	17	1.70 ± 0.38	31	44	1.34 ± 0.58
2C-3p+				31	44	2.01 ± 0.85
Logan	12	17	1.79 ± 0.39	31	44	1.43 ± 0.60
Logan+				31	44	2.26 ± 0.95

*Results are represented as mean ± SD. See Table 3 for conditions and definitions of abbreviations.

simplified model is similar to the previously reported rate constant for the conversion of ^{18}F-FDOPA to plasma OMFD: 0.024 ± 0.012 in the present study and 0.025 ± 0.019 in the 1991 study (*16*); this result suggests that our current k_3 value mainly reflects OMFD in tumor tissue that was transported from plasma. In other words, the non-zero k_3 value obtained with our current model (the question mark in Fig. 1) does not represent ^{18}F-FDOPA metabolism inside tumor cells.

The individual recovery coefficients were not measured with our PET system, but we used 0.7 for the transverse sinus and 1.0 for tumors, the striatum, and the cerebellum (*7*). With PET/CT scanners, correction for partial-volume effects can be performed on an individual basis. VOI generation may be simplified by generating VOIs directly from the high-resolution anatomic images fused to the metabolic images. FA remains important for the generation of time–activity curves because it highlights metabolically active and viable tissue. The threshold of 75% takes only the top quartile of voxels into account, that is, tumors with the most active metabolism. Necrotic zones have insufficient accumulation of ^{18}F-FDOPA and, therefore, do not reach 75% of the maximum accumulation in tumors. Areas with macroscopic necrosis are explicitly excluded during this VOI generation step. In the present study, the top quartile of voxels was selected to reduce fluctuations and to obtain a less noisy estimate of ^{18}F-FDOPA uptake relative to the maximum SUV estimated from one voxel. This method leads to more reliable fitting and parameter estimation. Parameters derived from this part of the tumor were correlated with the biology of the neoplasm, that is, high-grade tumors, low-grade tumors, or tumors with predominantly posttreatment changes (Fig. 5). Further studies with larger groups of patients are needed to confirm these observations.

Data obtained from the striatum of patients (Table 1) were different from data obtained from healthy volunteers (*16*). The values for k_1 and k_2 were 4 times higher and the values for k_3 and k_4 were 2 times higher in patients than in volunteers, whereas the distribution volumes were similar. These differences are related, in part, to our simplification of the original model of Huang et al. (*16*). On the other hand, these differences are not surprising, given the presence of tumors, possible medications (steroids), and therapy effects (radiation or chemotherapy) in patients. Although the k_4 value for the striatum was still low, the different absolute values of the parameter estimates obtained with the model in which k_4 was fixed at zero, and Patlak graphical analysis (Table 1), suggested that the k_4 value was not negligible. This suggestion, in turn, indicates that Patlak graphical analysis does not yield adequate estimates of ^{18}F-FDOPA kinetic parameters for the striatum of the diseased brain.

Tumor Kinetics and Biology

Figure 5 shows that high-grade tumors had the highest transport rate constant k_1. Significant differences ($P < 0.01$) between high- and low-grade tumors were found for k_1, k_2, K, SUV_{early}, and SUV_{late}. Comparison of high-grade tumors and tumors with predominantly posttreatment changes revealed significant differences for k_1, the blood volume fraction in tissue, SUV_{early}, and SUV_{late}. No significant differences in parameters were found between low-grade tumors and tumors with predominantly posttreatment changes. These findings suggest that high-grade tumors have overall higher transport rate and influx rate constants as well as higher early and late ^{18}F-FDOPA accumulation than do other tumor types.

Figure 4 and Tables 1 and 2 show that the mean k_3 value in the striatum was twice as high as those in malignant tumors and the cerebellum, whereas the k_4 values were the same. The interpretation of this finding is clear for the striatum, in which ^{18}F-FDOPA is converted to 6-fluorodopamine. The small values obtained for k_3 and k_4 in tumors and the cerebellum with our current model cannot be interpreted as bound ^{18}F-FDOPA in the third compartment but rather include metabolites in these brain structures, for example, tissue OMFD transported from plasma. A 2-compartment model appeared to be sufficient to describe ^{18}F-FDOPA kinetics in tumors and the cerebellum when plasma OMFD was not removed from the determination of the input function (i.e., without metabolite correction), at least as a first approximation. The combined activities of ^{18}F-FDOPA and OMFD measured by the PET scanner appeared to move in and out of tumor tissue and the cerebellum. The differences between the k_1 and k_2 values in tumors and the cerebellum could be attributed to differences in distribution volumes (Fig. 6). Logan graphical analysis produced reliable estimates of the distribution volumes for ^{18}F-FDOPA plus OMFD (Tables 3 and 4).

For all malignant tumors, the k_4 value was less than 0.07 min^{-1}. A weak correlation was found between the influx rate constants determined by Patlak graphical analysis and kinetic modeling (Pearson $r = 0.55$); the absolute value obtained by Patlak graphical analysis was about 25 times lower. This large and systematic difference indicates that when blood time–activity curves are not corrected for metabolites, the combined activities of ^{18}F-FDOPA and OMFD are not sequestered in tumor tissue.

These observations permit the formulation of a hypothesis regarding tumor kinetics. The available ^{18}F-labeled pool, that is, ^{18}F-FDOPA plus OMFD, is transported into tumor cells. This ^{18}F-labeled pool has a larger distribution volume in tumors than in the cerebellum, and the use of a 2-compartment model or Logan plots provides adequate estimates. When the ^{18}F-FDOPA fraction alone is considered, that is, when the input function is corrected for metabolites, a 3-compartment model is necessary to adequately describe the kinetics. In that case, the rate constant k_3 does not represent trapped ^{18}F-FDOPA in the third compartment but rather OMFD peripherally metabolized from ^{18}F-FDOPA and transported to the brain and into tumor cells. This notion is supported by the observation that the k_3 estimate for tumors was independent of the tumor grade (Fig. 5), comparable to that for the

cerebellum (no specific binding; Fig. 4), and similar to that for the peripheral conversion of ^{18}F-FDOPA to OMFD in normal volunteers (*16*). There is no indication that ^{18}F-FDOPA and OMFD are metabolized or trapped inside tumors. They stay in the amino acid pool, which is larger in tumors than in normal brain tissue (e.g., cerebellum and cortex), and are reflected in the increased radioactivity levels in tumors. The utility of OMFD as an amino acid analog for brain tumor imaging has been reported elsewhere (*20,26*). Thus, the increased uptake in tumors is an effect of the increased transport of and distribution volumes for amino acids and not the metabolism of ^{18}F-FDOPA inside tumor cells. For clinical purposes, the use of blood ^{18}F-FDOPA plus OMFD as the input function allows estimation of the transport rate and distribution volumes for amino acids in tumors (Tables 2 and 4).

Clinical Applications

In a previous clinical study (*8*), no differences in ^{18}F-FDOPA uptake were found between high- and low-grade tumors. This result has been reported for amino acid analogs, for example, methylmethionine, fluorotyrosine, and ^{18}F-FDOPA, by others (*2,3,27*). The similarity between high-grade tumor uptake and low-grade tumor uptake is usually interpreted as ^{18}F-FDOPA accumulation via a specific transport system (sodium-independent amino acid transport system L (*19*) but not system A (*28*)) rather than a breakdown of the BBB. This specific transport (*19*) and the low background activity (nonspecific amino acid uptake) explain the superiority of amino acid tracers over ^{18}F-FDG in evaluating tumor recurrence.

Differences in uptake between high-and low-grade tumors, however, have been reported for tyrosine (*29*) and ethyltyrosine (*30*). In the present study, a relationship between ^{18}F-FDOPA uptake and tumor grade was found. The main difference between the present study and the study of Chen et al. (*8*) relates to the timing and duration of imaging. In the study of Chen et al. (*8*), the images acquired from 10 to 30 min after tracer administration were summed (image duration, 20 min) and evaluated. In the present study, we found high variability in early uptake (~15 min), with a tendency for higher values for high-grade tumors but with a large overlap between tumor grades. Late uptake (~70 min), however, appeared to correlate better with influx rate constant K and was able to differentiate between high- and low-grade tumors. In an attempt to elucidate the optimal timing, the first derivative of the tumor uptake curve was calculated, and the initial steepest decline was determined. The maxima of the first derivative occurred, on average, at 28, 32, 37, and 33 min for high-grade tumors, low-grade tumors, tumors with predominantly posttreatment changes, and benign lesions, respectively. Except for 3 tumors, the maximum slope occurred within 40 min after tracer administration. These results suggest that for clinical applications, a shorter acquisition duration is sufficient to separate tumors. A 30-min study starting 15 min after ^{18}F-FDOPA administration and terminating at 45 min, with comparison of the SUVs at 20 and 40 min, should be sufficient to separate low- and high-grade tumors. For visual analysis, the entire 30-min study may be used to create images of high quality with low noise levels. Tumor uptake may be compared directly with uptake in the striatum, resulting in a sensitivity of 92% and a specificity of 95% for tumor recurrence, as reported earlier (*8*).

Given the much larger variations in SUV_{early} than in SUV_{late}, many of the sharp declines seen in high-grade tumors were averaged out (during image summation), leading to overall lower uptake and masking of high-grade tumors in the population. Current data revealed that high-grade tumors have higher and widely varying transport rates, with a rapid decline after the initial surge of ^{18}F-FDOPA uptake. These data suggest a breakdown of the BBB as an influx and efflux pathway in addition to specific transport through amino acid channels, as demonstrated earlier for ^{11}C-labeled methionine (*31*). In the previous clinical study (*8*), no differences in ^{18}F-FDOPA uptake were found between contrast-enhancing and nonenhancing tumors on MRI, suggesting that a BBB breakdown does not play a major role in ^{18}F-FDOPA levels in tumors. A further careful side-by-side comparison of dynamic contrast-enhanced MRI and dynamic ^{18}F-FDOPA PET is needed to elucidate the role of a BBB disruption and ^{18}F-FDOPA uptake in malignant tumors. Kinetic modeling suggests that ^{18}F-FDOPA and OMFD are transported into tumors and have different distribution volumes that are dependent on tumor grade and tumor type. In other words, tumors have different levels of uptake on PET images. The amino acids are transported into tumors and are not metabolized. This transport is probably mediated by amino acid transporters that are not very specific. Altered amino acid transport in tumors has been demonstrated with cell lines (*26,32–35*) and human tumors (*19,36*).

The limitations of our study include tumor heterogeneity, which resulted in small numbers of metastatic and benign lesions. Data for these tumor types need to be expanded. Robust effects were found for high-grade tumors, revealing significantly higher transport (k_1), influx (K), and equilibrium distribution volumes for these tumors than for other tumors. These differences were found for newly diagnosed tumors as well as recurrent tumors. On the other hand, no relationship was found between transport and influx for any of the tumor types.

CONCLUSION

^{18}F-FDOPA kinetics in brain tumors were investigated. FA was applied to provide image-derived blood clearance and tumor uptake curves that were not user dependent. A 3-compartment model with corrections for tissue blood volume, metabolites, and partial volume appeared to be adequate to describe the kinetics in the striatum, tumors, and the cerebellum. The same model structure was used for tumors, the striatum, and the cerebellum for reasons of

simplicity and the known applicability of the standard 3-compartment model for ^{18}F-FDG under clinical circumstances. Significant differences were found between high- and low-grade brain tumors in k_1 and K as well as in the equilibrium distribution volume. A high correlation was found between SUV_{late} in tumors and influx rate constant K, indicating that simple uptake measurements at 60–70 min should be sufficient in clinical practice, for example, for monitoring of the response to therapy.

ACKNOWLEDGMENT

This research was supported by DOE grant DE-FC02-02ER63420.

REFERENCES

1. Heiss WD, Wienhard K, Wagner R, et al. F-Dopa as an amino acid tracer to detect brain tumors. *J Nucl Med.* 1996;37:1180–1182.
2. Herholz K, Holzer T, Bauer B, et al. ^{11}C-Methionine PET for differential diagnosis of low-grade gliomas. *Neurology.* 1998;50:1316–1322.
3. Weber WA, Wester HJ, Grosu AL, et al. O-(2-[^{18}F]fluoroethyl)-L-tyrosine and L-[methyl-^{11}C]methionine uptake in brain tumours: initial results of a comparative study. *Eur J Nucl Med.* 2000;27:542–549.
4. Jager PL, Vaalburg W, Pruim J, de Vries EG, Langen KJ, Piers DA. Radiolabeled amino acids: basic aspects and clinical applications in oncology. *J Nucl Med.* 2001;42:432–445.
5. Becherer A, Karanikas G, Szabo M, et al. Brain tumour imaging with PET: a comparison between [^{18}F]fluorodopa and [^{11}C]methionine. *Eur J Nucl Med Mol Imaging.* 2003;30:1561–1567.
6. Chen W, Cloughesy T, Kamdar N, et al. Imaging proliferation in brain tumors with ^{18}F-FLT PET: comparison with ^{18}F-FDG. *J Nucl Med.* 2005;46:945–952.
7. Schiepers C, Chen W, Dahlbom M, Cloughesy T, Hoh CK, Huang SC. ^{18}F-Fluorothymidine kinetics of malignant brain tumors. *Eur J Nucl Med Mol Imaging.* 2007;34:1003–1011.
8. Chen W, Silverman DH, Delaloye S, et al. ^{18}F-FDOPA PET imaging of brain tumors: comparison study with ^{18}F-FDG PET and evaluation of diagnostic accuracy. *J Nucl Med.* 2006;47:904–911.
9. Huang SC, Barrio JR, Yu DC, et al. Modelling approach for separating blood time-activity curves in positron emission tomographic studies. *Phys Med Biol.* 1991;36:749–761.
10. Patlak CS, Blasberg RG. Graphical evaluation of blood-to-brain transfer constants from multiple-time uptake data: generalizations. *J Cereb Blood Flow Metab.* 1985;5:584–590.
11. Logan J, Fowler JS, Volkow ND, et al. Graphical analysis of reversible radioligand binding from time-activity measurements applied to [N-^{11}C-methyl]-(−)-cocaine PET studies in human subjects. *J Cereb Blood Flow Metab.* 1990;10:740–747.
12. Namavari M, Bishop A, Satyamurthy N, Bida G, Barrio JR. Regioselective radiofluorodestannylation with [^{18}F]F2 and [^{18}F]CH3COOF: a high yield synthesis of 6-[^{18}F]fluoro-L-dopa. *Int J Rad Appl Instrum [A].* 1992;43:989–996.
13. Nuyts J, Baete K, Beque D, Dupont P. Comparison between MAP and postprocessed ML for image reconstruction in emission tomography when anatomical knowledge is available. *IEEE Trans Med Imaging.* 2005;24:667–675.
14. Nuyts J, Michel C, Dupont P. Maximum-likelihood expectation-maximization reconstruction of sinograms with arbitrary noise distribution using NEC-transformations. *IEEE Trans Med Imaging.* 2001;20:365–375.
15. Schiepers C, Hoh CK, Nuyts J, Wu HM, Phelps ME, Dahlbom M. Factor analysis in prostate cancer: delineation of organ structures and automatic generation of in- and output functions. *IEEE Trans Nucl Sci.* 2002;49:2338–2343.
16. Huang SC, Yu DC, Barrio JR, et al. Kinetics and modeling of L-6-[^{18}F]fluoro-dopa in human positron emission tomographic studies. *J Cereb Blood Flow Metab.* 1991;11:898–913.
17. Phelps ME, Huang SC, Hoffman EJ, Selin C, Sokoloff L, Kuhl DE. Tomographic measurement of local cerebral glucose metabolic rate in humans with (F-18)2-fluoro-2-deoxy-D-glucose: validation of method. *Ann Neurol.* 1979;6:371–388.
18. Huang SC, Phelps ME, Hoffman EJ, Sideris K, Selin CJ, Kuhl DE. Noninvasive determination of local cerebral metabolic rate of glucose in man. *Am J Physiol.* 1980;238:E69–E82.
19. Langen KJ, Broer S. Molecular transport mechanisms of radiolabeled amino acids for PET and SPECT. *J Nucl Med.* 2004;45:1435–1436.
20. Beuthien-Baumann B, Bredow J, Burchert W, et al. 3-O-Methyl-6-[^{18}F]fluoro-L-DOPA and its evaluation in brain tumour imaging. *Eur J Nucl Med Mol Imaging.* 2003;30:1004–1008.
21. Draper NR, Smith H. *Applied Regression Analysis*. 2nd ed. New York, NY: John Wiley & Sons; 1981.
22. Landaw EM, DiStefano JJ III. Multiexponential, multicompartmental, and noncompartmental modeling. II. Data analysis and statistical considerations. *Am J Physiol.* 1984;246:R665–R677.
23. Wu HM, Hoh CK, Choi Y, et al. Factor analysis for extraction of blood time–activity curves in dynamic FDG-PET studies. *J Nucl Med.* 1995;36:1714–1722.
24. Schiepers C, Hoh CK, Seltzer MA, Phelps ME, Dahlbom M. Factor analysis for quantification of ^{11}C-acetate PET in primary prostate cancer [abstract]. *J Nucl Med.* 2000;41(5 suppl):100P.
25. Schiepers C, Czernin J, Hoh CK, Nuyts J, Phelps ME, Dahlbom M. Factor analysis for automatic determination of myocardial flow in ^{13}N-ammonia PET studies [abstract]. *J Nucl Med.* 2002;43(5 suppl):52P.
26. Bergmann R, Pietzsch J, Fuechtner F, et al. 3-*O*-Methyl-6-^{18}F-fluoro-L-dopa, a new tumor imaging agent: investigation of transport mechanism in vitro. *J Nucl Med.* 2004;45:2116–2122.
27. Pauleit D, Floeth F, Hamacher K, et al. O-(2-[^{18}F]Fluoroethyl)-L-tyrosine PET combined with MRI improves the diagnostic assessment of cerebral gliomas. *Brain.* 2005;128:678–687.
28. Sutinen E, Jyrkkio S, Gronroos T, Haaparanta M, Lehikoinen P, Nagren K. Biodistribution of [^{11}C] methylaminoisobutyric acid, a tracer for PET studies on system A amino acid transport in vivo. *Eur J Nucl Med.* 2001;28:847–854.
29. Wienhard K, Herholz K, Coenen HH, et al. Increased amino acid transport into brain tumors measured by PET of L-(2-^{18}F)fluorotyrosine. *J Nucl Med.* 1991;32:1338–1346.
30. Popperl G, Kreth FW, Herms J, et al. Analysis of ^{18}F-FET PET for grading of recurrent gliomas: is evaluation of uptake kinetics superior to standard methods? *J Nucl Med.* 2006;47:393–403.
31. Roelcke U, Radu EW, von Ammon K, Hausmann O, Maguire RP, Leenders KL. Alteration of blood-brain barrier in human brain tumors: comparison of [^{18}F]fluorodeoxyglucose, [^{11}C]methionine and rubidium-82 using PET. *J Neurol Sci.* 1995;132:20–27.
32. Miyagawa T, Oku T, Uehara H, et al. "Facilitated" amino acid transport is upregulated in brain tumors. *J Cereb Blood Flow Metab.* 1998;18:500–509.
33. Sasajima T, Miyagawa T, Oku T, Gelovani JG, Finn R, Blasberg R. Proliferation-dependent changes in amino acid transport and glucose metabolism in glioma cell lines. *Eur J Nucl Med Mol Imaging.* 2004;31:1244–1256.
34. Isselbacher KJ. Increased uptake of amino acids and 2-deoxy-D-glucose by virus-transformed cells in culture. *Proc Natl Acad Sci USA.* 1972;69:585–589.
35. Isselbacher KJ. Sugar and amino acid transport by cells in culture: differences between normal and malignant cells. *N Engl J Med.* 1972;286:929–933.
36. Hatazawa J, Ishiwata K, Itoh M, et al. Quantitative evaluation of L-[methyl-C-11] methionine uptake in tumor using positron emission tomography. *J Nucl Med.* 1989;30:1809–1813.

JNM The Journal of NUCLEAR MEDICINE

^{18}F-FDOPA Kinetics in Brain Tumors

Christiaan Schiepers, Wei Chen, Timothy Cloughesy, Magnus Dahlbom and Sung-Cheng Huang

J Nucl Med. 2007;48:1651-1661.
Published online: September 14, 2007.
Doi: 10.2967/jnumed.106.039321

The Journal of Nuclear Medicine is published monthly.
SNMMI | Society of Nuclear Medicine and Molecular Imaging
1850 Samuel Morse Drive, Reston, VA 20190.
(Print ISSN: 0161-5505, Online ISSN: 2159-662X)

SNMMI SOCIETY OF NUCLEAR MEDICINE AND MOLECULAR IMAGING